PCCP

PAPER

View Article Online
View Journal | View Issue

Cite this: *Phys. Chem. Chem. Phys.*, 2023, **25**, 11697

Electronic structure of rhombus-shaped nanographenes: system size evolution from closed- to open-shell ground states†

M. E. Sandoval-Salinas, R. Bernabeu-Cabañero, A. J. Pérez-Jiménez, E. San-Fabián and J. C. Sancho-García *

We theoretically study and characterize a set of rhombus-shaped nanographenes of increasing size, or *n*-rhombenes, where *n* = 2–6, displaying zigzag edges leading to an enhancement of the (poly)radicaloid nature and the appearance of intrinsic magnetism as a function of *n*. Due to that system-dependent radicaloid nature, we employ spin-flip methods able to capture the challenging physics of the problem, thus providing accurate energy differences between high- and low-spin solutions. The theoretical predictions agree with the experimentally available magnetic exchange coupling for the recently synthesized 5-rhombene, as well as with the size at which the transition from a closed-shell to an open-shell ground-state solution occurs. We also investigate if standard DFT methods are able to reproduce the trend disclosed by spin-flip methods and if the results are highly dependent on the functional choice and/or the intrinsic spin contamination.

Received 10th March 2023,
Accepted 4th April 2023

DOI: 10.1039/d3cp01103h

rsc.li/pccp

1. Introduction

There is an increasing interest[1–7] on open-shell graphene structures (*i.e.*, nanometer-sized flat graphene nanoforms such as nanoflakes, nanoislands, *etc.*) with tailored edges and sizes, due to several factors, namely: (i) the dependence of total and local magnetism on the particular topology (*e.g.* shape and/or sublattice imbalance) of the systems, theoretically predicted time ago;[8–10] and (ii) the recent advances in atomically-induced open-shell nanographene synthesis of a variety of these challenging nanoforms.[11–15] As part of these research interests, we will consider in this study a family of graphene nanoforms displaying a rhombus shape arising from fusing two triangular fragments, with the chemical formula $C_{2n^2+4n}H_{4n+2}$ and dubbed as *n*-rhombenes, with *n* indicating the system size (Fig. 1). More specifically, *n* is the number of benzenoid rings along any of both edges. These systems are predicted to have a singlet ($S = 0$) ground state following the Ovchinnikovs rule[16] and its latter generalization known as Lieb's theorem,[17] given that for these molecules an equal number of C atoms holds in the two interprenetating sublattices in which the topological structure can be decomposed. However, the closed- or open-shell nature of that singlet state might be highly dependent on the size, as well as the energy position of other high-lying states, which also prompted previous theoretical investigations.[18–20]

Going into more details, the smallest member of the family (*i.e.*, 2-rhombene or benzo[def]phenanthrene, simply known as pyrene) has been synthesized time ago,[21] and it is also found on

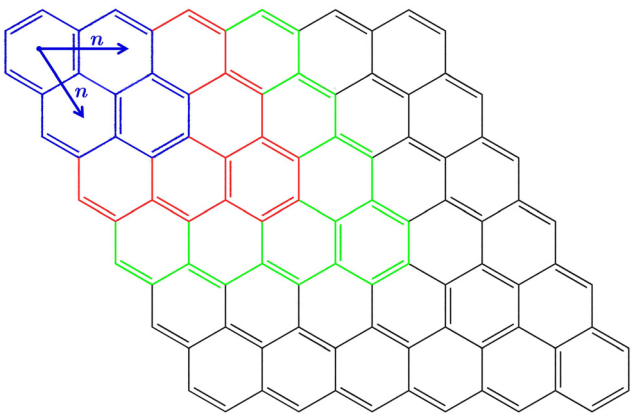

Fig. 1 Chemical structures of the *n*-rhombenes studied (H atoms are not shown).

Department of Physical Chemistry, University of Alicante, E-03080 Alicante, Spain. E-mail: jc.sancho@ua.es

† Electronic supplementary information (ESI) available: (i) IR spectra of *n*-rhombenes; (ii) plots of the $\rho_U(\mathbf{r})$ spatial distribution of *n*-rhombenes; (iii) N_U and Y_i values calculated at the RAS-SF/6-31G* level for *n*-rhombenes; (iv) HOMO and LUMO orbital energies as calculated at various DFT/def2-TZVP levels; (v) vertical singlet–triplet and singlet–quintet energies calculated at the RAS-SF/6-31G* and DFT/def2-TZVP levels for *n*-rhombenes; (vi) $\langle \hat{S}2 \rangle$ values for singlet, triplet, and quintet states at the DFT level; (vii) plots of the (triplet and open-shell singlet) spin density spatial distribution of *n*-rhombenes; (viii) cartesian coordinates of *n*-rhombenes optimized at the B97-3c level. See DOI: **https://doi.org/10.1039/d3cp01103h**

interstellar searches,[22] used as template for metal–organic frameworks,[23] or for fusing other acenes and azaacenes,[24] to name just a few examples of its chemical versatility and functionality. Note also that the synthesis of other members of the family had not been reported, possibly due to the increase of their polyradicaloid (or open-shell) character mentioned above, until the emergence of new atomic-scale techniques allowing their experimental realization. Actually, the surface-assisted synthesis of 4-rhombene and 5-rhombene on Au(111) was very recently reported in ref. 25, further characterized by Scanning Tunneling Microscopy (STM) and probed by inelastic electron tunnelling spectroscopy (IETS) and differential conductance spectroscopy measurements. Those experiments revealed a closed-shell singlet (S = 0) ground-state for 4-rhombene but an open-shell singlet for 5-rhombene, separated by 102 meV from a low-lying triplet (S = 1) state, in agreement with various calculations carried out concomitantly to that experimental investigation.[26]

However, there are still a few questions that can be treated from a computational point of view regarding these systems, as well as the evolution of electronic properties as a function of the system size, namely: the degree of (poly)radicaloid character and its characterization in terms of the number and distribution of unpaired electrons, the impact of spin contamination on the computational results, the evolution of the magnetic exchange coupling, the energy location of other viable high-spin states such as the quintet, the energy needed to oxidize and reduce the molecules, *etc.* Additionally, the use of standard Density Functional Theory (DFT) on these systems is not exempted from difficulties,[27,28] due to the increasing open-shell character with n, unless using some non-standard extensions to deal with fractional occupation of molecular orbitals.[29] The main goal of the present study is to address these open questions by means of electronic structure calculations. Nevertheless, to circumvent these difficulties and obtain highly accurate results to be taken as reference, we will also apply here more time-intensive and sophisticated methods such as the Restricted Active Space Spin-Flip (RAS-SF) method,[30–32] which has been previously demonstrated to be a reliable tool to obtain very accurate results for (poly)radicaloid compounds.[33] The RAS-SF will also be coupled[34] with a short-range exchange–correlation energy functional (RAS-srDFT) to incorporate in a balanced way dynamical (or short-range) and non-dynamical (or long-range) correlation effects.[35,36] Therefore, we will study the set of n-rhombenes, with n = 2–6, to address not only the evolution of electronic properties with the system size but also to simultaneously assess the accuracy of the methods chosen.

2. Theoretical framework

The characterization of the (poly)radicaloid nature of these compounds will be first estimated by the fractional occupation of molecular orbitals induced by (near-)degeneracy effects, which in open-shell systems can be simulated by minimizing the Gibbs electronic free energy ($G_{el} = E_{el} - T_{el}S_{el}$) of the system, at a fictitious pseudo-temperature (*i.e.*, electronic) called T_{el} and imposing a Fermi–Dirac distribution around the Fermi level E_F:

$$f_i = \frac{1}{1 + e^{(\varepsilon_i - E_F)/\theta}}, \quad (1)$$

with f_i being the fractional occupation numbers, and $\theta = k_B T_{el}$. This kind of methods are collectively denoted as Finite–Temperature DFT (FT-DFT).[37–39]

Reference values for energy differences between singlet (S), triplet (T), and quintet (Q) spin states (*vide infra*) will be obtained by the Restricted Active Space Spin-Flip (RAS-SF) method, allowing multiple spin-flip excitations[40] within the active space chosen of doubly occupied (RAS1), singly occupied (RAS2), and virtual (RAS3) subspaces. The RAS-SF Hamiltonian is defined as that of n-spin-flip excitations expanded in terms of the number of holes (particles) in the doubly occupied (virtual) space:

$$\hat{R}^{nSF} = \hat{r}_0^{nSF} + \hat{r}_h^{nSF} + \hat{r}_p^{nSF} + \hat{r}_{hp}^{nSF} + \hat{r}_{2h}^{nSF} + \hat{r}_{2p}^{nSF} + \ldots, \quad (2)$$

where $\hat{r}_0^{nSF}$ performs all possible spin-flip excitations within RAS2 and h and p subindices indicate the number of holes and particles in RAS1 and RAS3, respectively. In the approximation used here $p = h = 1$; *i.e.*, the right side of eqn (2) is truncated at the third term. The eigenvalues are obtained from a wavefunction expanded over a high-spin single reference restricted set of Slater determinants, $|\Psi^{RAS}\rangle = \sum_R C_R|\Phi_R\rangle$, where $|\Phi_R\rangle$ are the allowed electronic configurations. These calculations will be also coupled with the PBE[41] short-range exchange–correlation energy functional, to introduce both types (long- and short-range) of electron correlation effects, briefly denoted as RAS-srPBE in the following, since this functional is chosen for this RAS-srDFT extension.

The relative energies between those low-lying and different spin states will also be obtained by Density Functional Theory (DFT), employing semi-local and both Global–Hybrid (GH) and Double–Hybrid (DH) density functionals, to bracket if the accuracy of the calculations depends on the choice of the exchange–correlation functional. The general expression for a GH functional is given by:

$$E_{xc}^{GH}[\rho] = c_x E_x^{EXX} + (1 - c_x)E_x[\rho] + E_c[\rho], \quad (3)$$

with the exchange contribution being a linear function of the EXact-eXchange (EXX) energy, E_x^{EXX}, and the exchange functional, $E_x[\rho]$, weighted by a coefficient c_x (note that for a semi-local functional $c_x = 0$). This expression can be extended to a DH form as:

$$E_{xc}^{DH}[\rho] = c_x E_x^{EXX} + (1 - c_x)E_x[\rho] + c_c E_c^{PT2} + (1 - c_c)E_c[\rho], \quad (4)$$

that is, adding the 2nd-order Perturbation Theory energy, E_c^{PT2}, to the correlation functional, $E_c[\rho]$, weighted now by the coefficient c_c. The expressions for:

$$E_x^{EXX} = -\frac{1}{2}\sum_{ij}^{N}\iint \phi_i^*(\mathbf{r})\phi_j^*(\mathbf{r}')\frac{1}{|\mathbf{r} - \mathbf{r}'|}\phi_j(\mathbf{r})\phi_i(\mathbf{r}')d\mathbf{r}d\mathbf{r}', \quad (5)$$

$$E_c^{PT2} = \frac{1}{4}\sum_{i,j}^{N}\sum_{a,b}^{M}\frac{|\langle ab||ij\rangle|^2}{(\varepsilon_a+\varepsilon_b)-(\varepsilon_i+\varepsilon_j)}, \quad (6)$$

with $\langle ab||ij\rangle = \langle ab|ij\rangle - \langle ab|ji\rangle$, rely both on the set of occupied ($\{\phi_i\}$) and virtual ($\{\phi_a\}$) orbitals self-consistently generated by eqn (3) and used hereinafter. We will select for these calculations the semi-local PBE[41] ($c_x = 0$), the hybrid PBE0[42] ($c_x = 1/4$) and PBEHH ($c_x = 1/2$), and the double-hybrid PBE0-DH[43] ($c_x = 1/2$ and $c_c = 1/8$) exchange–correlation functionals, all of them belonging to the same non-empirical family of expressions but differing in their hybridization.[44,45] Furthermore, a Broken–Symmetry (BS) solution will also be carefully obtained at all those levels for the corresponding open-shell singlet states.

The spin-contamination associated to DFT calculations can be reduced to better estimate the singlet–triplet and singlet–quintet energy differences, or ΔE_{ST} and ΔE_{SQ}, respectively. Denoting the low-spin ($M_s = 0$) and high-spin (*e.g.* $M_s = 1$ for a triplet) solutions as LS and HS, respectively, one of the simplest forms has been proposed by Yamaguchi *et al.*[46–48] exploiting the difference between the calculated mean values of the $\hat{S}^2$ spin operator for the two solutions involved, such as:

$$\Delta E(\mathrm{HS} - \mathrm{LS}) = \delta\cdot[E(\mathrm{HS}) - E(\mathrm{LS})], \quad (7)$$

with:

$$\delta = \frac{n_S}{\langle\hat{S}^2\rangle_{HS} - \langle\hat{S}^2\rangle_{LS}} \quad (8)$$

where n_S corresponds to the $\langle\hat{S}^2\rangle$ difference between the ideal spin eigenvalues, *e.g.*, $n_S = 2$ for a singlet–triplet. In the case of *n*-rhombenes, we will calculate ΔE_{ST} and ΔE_{SQ} values, with S, T, and Q corresponding to the lowest-energy solutions fixing $M_s = 0$ (singlet), $M_s = 1$ (triplet), and $M_s = 2$ (quintet) or, in other words, the $S_0 - T_1$ and $S_0 - Q_1$ energy difference. In the case of the singlet states, an open-shell solution will also be imposed which will be used to calculate those ΔE_{ST} and ΔE_{SQ} values and thus infer for which value of n the closed- and open-shell solutions might differ.

2.1 Computational details

The geometries of the compounds are initially optimized by the B97-3c method[49] leading to planar structures identified by all-real $3N - 6$ vibrational frequencies. The FT-DFT calculations are done with the recommended TPSS[50] functional and the default temperature of 5000 K, together with the def2-TZVP basis set,[51] employing the ORCA 5.0 package.[52] The spatial plots of $\rho_U(\mathbf{r})$ are done with the AVOGADRO 1.97 visualizer.[53] The same ORCA 5.0 package is also used for the DFT calculations with different exchange–correlation functionals and the def2-SVP and def2-TZVP basis sets. The RIJCOSX technique,[54] together with the auxiliary def2/JK and def2-*n*VP/C basis sets,[55] is fixed for the latter calculations to alleviate the computational cost. The cc-pVTZ basis set is also used for some test calculations, employing again the corresponding auxiliary basis sets. For the RAS-SF calculations, done here with the Q-CHEM 6.0 package,[56] we also assess the dependence of the results with respect to different basis sets (6-31G*, 6-311G*, def2-SVP, and def2-TZVP). For the RAS-based calculations, the number of electrons (N_e) in the number of active orbitals (N_o), or briefly (N_e,N_o), is chosen consistently with the fractional occupation disclosed at the FT-DFT level, that is, (4,4) for 2-rhombene, (6,6) for 3-rhombene, and (10,10) for the rest of *n*-rhombenes (4- to 6-rhombene). A triplet state was used as the high-spin reference for RAS-SF, except for $n = 5$–6 for which a quintet state was instead used.

3. Results and discussion

3.1 Geometrical features

The B97-3c optimized geometry for the 2-rhombene molecule, the only system for which X-ray data exists,[57] are in close agreement with the experimental results (averaged error of 0.0080 Å) and very close to those calculated for consistency at the PBE0/def2-TZVP and PBE0-DH/def2-TZPV levels (averaged errors of 0.0065 and 0.0062 Å, respectively) which are known to be very accurate methods for geometry optimizations.[58] The Bond Length Alternation (BLA) can be calculated by B97-3c to estimate the average difference in lengths between single and double bonds along the zigzag edges:[59]

$$\mathrm{BLA} = \frac{1}{N-2}\sum_{i=1}^{N-2}(-1)^{i+1}\left(d_{i+1,i+2} - d_{i,i+1}\right), \quad (9)$$

where $d_{i,j}$ is the distance between atoms i and j out of the N total C atoms. BLA values (in Å, as calculated at the B97-3c level) of 0.029, 0.033, 0.031, 0.027, and 0.023, are found from 2-rhombene to 6-rhombene, respectively, indicating only slight variations of aromaticity as a function of the system size n. Note also that these values are lower than those found before[60] for oligoacetylenes of similar length, as it is also expected from the extended conjugation of the (fully planar) *n*-rhombenes. The same trend for BLA values is reproduced by PBE0/def2-SVP or PBE0/def2-TZVP methods, with the latter giving slightly higher values (in Å) of 0.034, 0.041, 0.040, and 0.036 for 2- to 5-rhombene, respectively. The InfraRed (IR) spectra of the set of *n*-rhombenes, at the B97-3c level, shows (see the ESI†) pronounced peaks at $\approx$850 and $\approx$3130 cm^{-1} for the CH out-of-plane bending and CH stretching, respectively, whose intensity progressively increases with the system size and thus with the number of CH bonds, in agreement with the expected results for polycyclic aromatic hydrocarbons.[61]

3.2 The (poly)radicaloid character of the systems

A simple yet effective estimate of the radicaloid character is obtained by the FT-DFT method, providing the energy distribution of electrons around the Fermi level, which can also be represented as a spatial density:

$$\rho_U(\mathbf{r}) = \sum_i f_i|\{\varphi_i(\mathbf{r})\}_U|^2, \quad (10)$$

with f_i being the fractional occupation number ($0 < f_i < 2$) corresponding to that subset of orbitals ($\{\varphi_i\}_U$) holding a fractional occupation. The integration of $\rho_U(\mathbf{r})$ directly leads

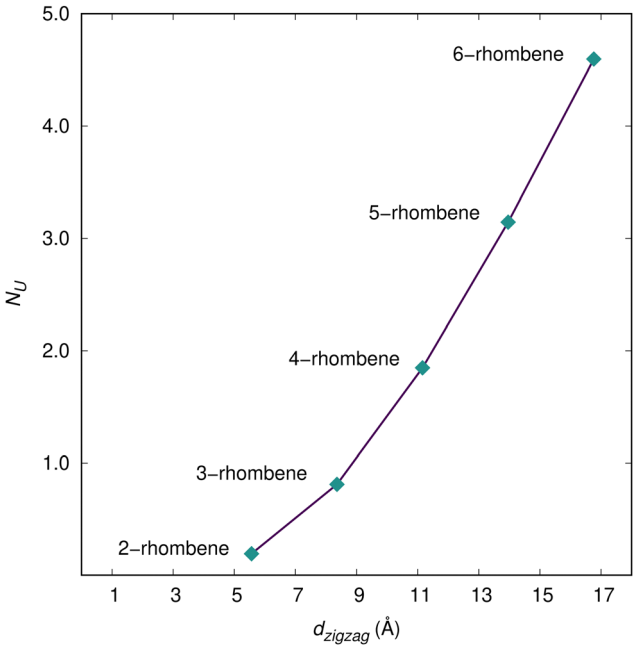

Fig. 2 Evolution of the N_U values of n-rhombenes, as calculated by the FT-TPSS/def2-TZVP method, as a function of the zigzag length (in Å) measured as the sum of the ($2n$) CC bond lengths along one of the four (symmetrical) edges of the systems.

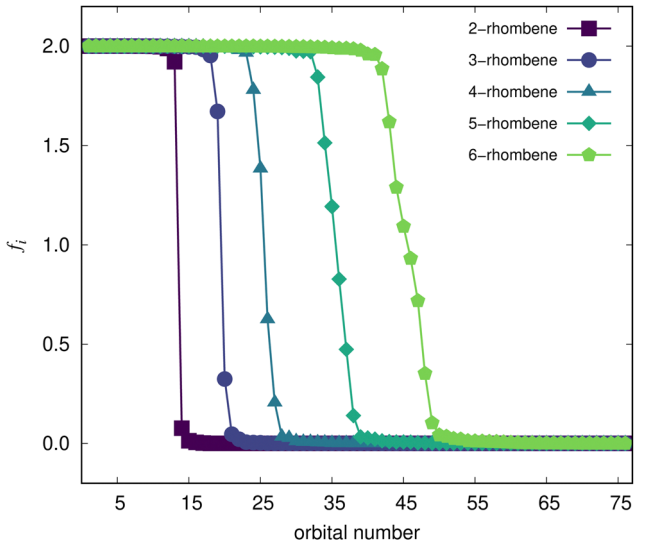

Fig. 3 Orbital occupation numbers (f_i) of n-rhombenes, as calculated by the FT-TPSS/def2-TZVP method.

to N_U, a global measure of the number of strongly correlated electrons. The N_U values for the (singlet) ground-state of n-rhombenes are 0.19, 0.81, 1.85, 3.14, and 4.60 for 2-rhombene, 3-rhombene, 4-rhombene, 5-rhombene, and 6-rhombene, respectively, increasing significantly with the system size as it does also the length of the zigzag edges (see Fig. 2). This relationship can be easily understood by the real-space distribution of $\rho_U(\mathbf{r})$, see the ESI,† which is strongly localized at those C atoms belonging to the zigzag edges, taking also into account that $\rho_U(\mathbf{r})$ (and thus N_U) is a size-extensive magnitude. This topology of $\rho_U(\mathbf{r})$ agrees with the distribution found before for other graphene nanoribbons[62] or linear and cyclic oligoacenes.[63]

The evolution of the ground-state fractional occupation numbers through the n-rhombenes family is presented in Fig. 3, which includes now a large manifold of orbitals to better appreciate how the (poly)radicaloid nature evolves with the system size. It is immediately apparent that the number of orbitals with fractional occupation increases with the system size, with the ground-state of smaller n-rhombenes ($n \leq 3$) displaying a vanishing or small diradicaloid character, consistent with the information available in the literature for *e.g.* pyrene.[64] On the other hand, the larger n-rhombenes tackled here (*i.e.*, 4-rhombene, 5-rhombene, and 6-rhombene) exhibited a more marked diradicaloid character, with a larger number of orbitals with occupation $f_i \approx 1$, which is also in agreement with the larger N_U values found from $\rho_U(\mathbf{r})$. Overall, the largest n-rhombenes should be considered as of a significantly (poly)radicaloid nature.

Additionally, the degree of the (poly)radicaloid character of the compounds can also be estimated by the radical indexes Y_i number[65] (i = 0, 1, 2) generally obtained as $Y_i = f_{\mathrm{LUNO}+i}$, with f_{LUNO} being the fractional occupation number of the Lowest Unoccupied Natural Orbital. For a N-electron system, the Highest Occupied Natural Orbital (HONO) is defined as the (N/2)th orbital while the Lowest Unoccupied Natural Orbital (LUNO) is defined as the (N/2 + 1)th orbital, with the rest of orbitals defined correspondingly. At the RAS-SF/6-31G* level, we obtain values for each of the Y_0, Y_1, and Y_2 index, which are respectively related to the di-, tetra-, and hexa-radicaloid character. Note that $Y_i \approx 1$ suggests a high radical character (*e.g.* $Y_0 = 0$ for a closed-shell system and $Y_0 = 1$ for a diradical). Fig. 4 shows the Y_i values for the set of n-rhombenes, indicating a low radicaloid character for 2- and 3-rhombene, a moderate diradicaloid character for 4-rhombene, and a low to moderate tetraradicaloid character for the largest 5- and 6-rhombene. This conclusion is in qualitative agreement with previous and simplified topological approaches for the treatment of conjugated hydrocarbons.[66]

3.3 Singlet–triplet and singlet–quintet energy gap

3.3.1 Results from wavefunction methods. First of all, we will assess for 2- and 3-rhombene RAS-based methodological aspects to better bracket the accuracy of the RAS-SF results for the rest of the largest systems. The use of a large (def2-TZVP) or a cost-effective (6-31G*) basis set brings only a small difference for the target ΔE(HS − LS) values, that is ΔE_{ST} and ΔE_{SQ} energy differences: Going from def2-TZVP to 6-31G* modifies for 2-rhombene (3-rhombene) the ΔE_{ST} value by 0.05 (0.08) eV, while ΔE_{SQ} was affected by 0.14 (−0.01) eV. In this comparison, we will also include next the RAS-srPBE/6-31G* results for which, similarly, the ΔE_{ST} and ΔE_{SQ} values are only slightly affected, as can be seen in Fig. 5 summarizing the impact of these technical aspects on the results. Therefore, we will rely in the following on the cost-effective RAS-SF/6-31G* results for the largest (and more challenging) n-rhombenes as a good compromise between accuracy and computational cost.

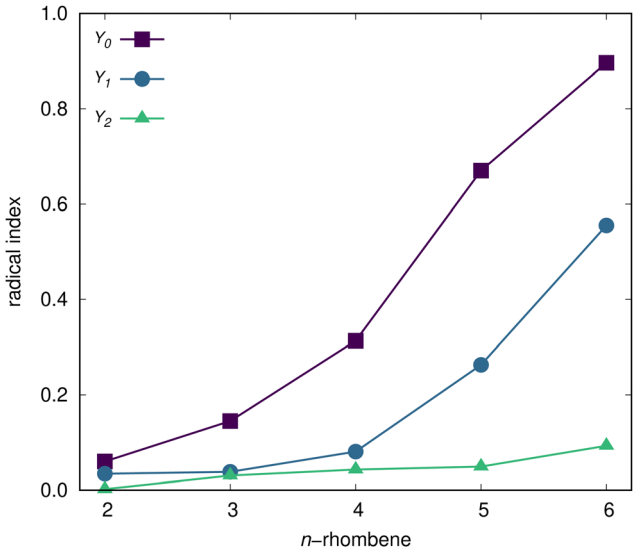

Fig. 4 Radical index (Y_i) of n-rhombenes, as calculated by the RAS-SF/6-31G* method.

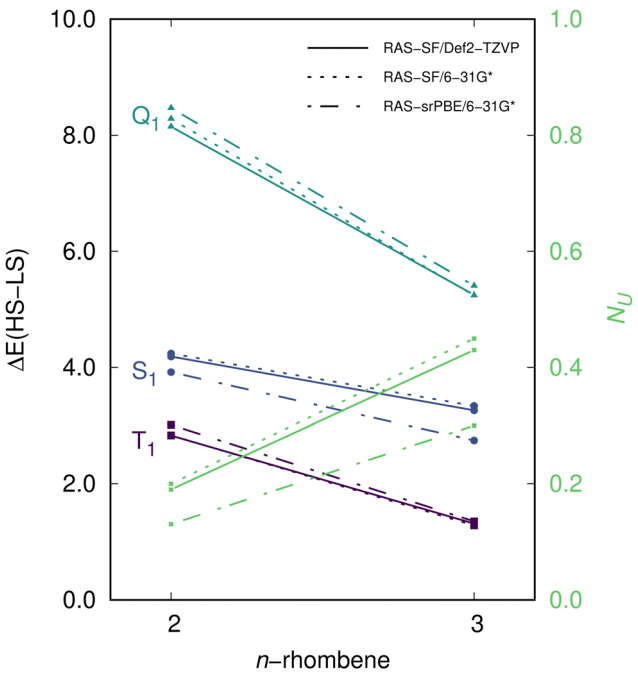

Fig. 5 Energy difference (in eV) between the low- and high-spin states of 2- and 3-rhombene, and N_U, as calculated at various RAS-based theoretical levels.

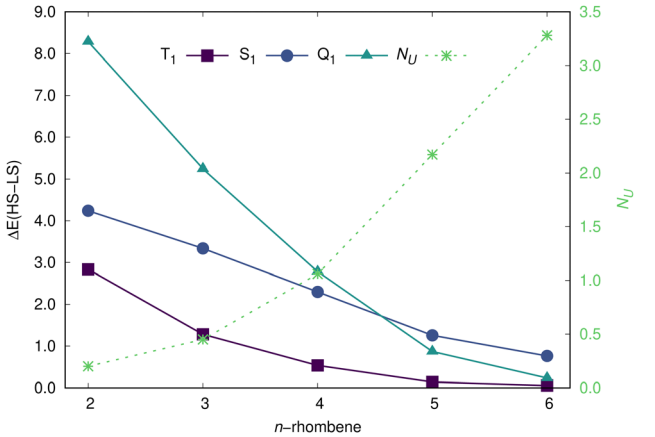

Fig. 6 Energy difference (in eV) between the low- and high-spin states of n-rhombenes, and N_U, as calculated by the RAS-SF/6-31G* method.

The evolution of ΔE_{ST} and ΔE_{SQ} values with the system size is presented in Fig. 6, with both energy differences smoothly decreasing as a function of n (for completeness, the figure also includes the S_1 state). The smaller systems, 2- to 4-rhombene, keep a substantial energy difference between low-spin and high-spin (be T_1 or Q_1) states, which is fully consistent with their low radicaloid character. For the longest rhombenes, the ΔE_{ST} and ΔE_{SQ} values are considerably lower, with the T_1 state being always the lowest one. Actually, for the case of 5-rhombene, the T_1 state is energetically predicted (RAS-SF/6-31G* level) at 139 meV above the (open-shell) S_0 state, in close agreement with the experimentally determined energy difference between those states of 102 meV[25] (note that the surface is known to play a negligible influence to adequatly compare experimental and calculated values according to recent studies[67]). For 6-rhombene, that ΔE_{ST} values slightly decreases to 56 meV, a value still few times larger than the Landauer limit[68] [*i.e.*, $k_B T \ln(2) \approx 18$ meV, with k_B the Boltzmann constant and T the temperature] for energy dissipation at room temperature, a key magnitude for having stable spintronics devices. Note that for 6-rhombene, the ΔE_{ST} and the ΔE_{SQ} values are energetically close just separated by less than 0.2 eV.

The results by RAS-SF/6-31G* will also be compared for 4- to 6-rhombenes with those obtained using (Strongly-Contracted) *N*-electron Valence second-order Perturbation Theory or (SC-)NEVPT2,[69–71] as a sanity check given the high accuracy of the latter method for related systems,[72] employing the same active space (10,10) and basis set than for RAS-SF. Interestingly, the T_1 state for 5-rhombene (6-rhombene) is also found lying 139 (75) meV above the S_0 state, in perfect agreement with the RAS-SF results. Finally, other results from literature are compared here for the sake of completeness: (i) NEVPT2/STO-3G calculations[73,74] led to negligible ΔE_{ST} values of 16 and 3 meV for 5- and 6-rhombene, respectively, and too low ΔE_{SQ} values too, thus indicating the need of more realistic basis sets; and (ii) TAO-LDA calculations[64] reported ΔE_{ST} values for 4- to 6-rhombene of 440, 204, and 116 meV, closely following the trend of the values calculated here although slightly overestimating the experimental result for 5-rhombene.

3.3.2 Assessment of DFT methods. A simple yet useful estimate of the performance of the PBE-based functionals (all calculations are done with the def2-TZVP basis set unless otherwise noticed) will be the comparison of the results with the experimentally available HOMO–LUMO gap (0.73 eV) of 4-rhombene. Due to the fact that the ground-state of 4-rhombene is experimentally predicted to be a closed-shell system, the closest estimate is provided by PBE (0.66 eV)

followed by PBE0 (1.36 eV) and PBEHH (2.13 eV), thus indicating that a relatively low c_x weight [see eqn (3)] is favoured in this case. Actually, a calculation with an *ad hoc* PBEh hybrid functional[75] (for which $c_x = 1/10$) leads to an intermediate value of 0.93 eV between those calculated by PBE and PBE0, showing how (linearly) dependent the HOMO–LUMO gap with respect to c_x is. This finding prompts us to discard PBEHH (the functional with the highest c_x weight) for the rest of the calculations shown here.

The FT-DFT method will be first applied for a fast estimate of the ΔE_{ST} (ΔE_{SQ}) energy differences, with calculated values (all in eV) of 1.864, 0.869, 0.430, 0.255, and 0.174 (5.239, 3.115, 1.792, 1.095, 0.741) and thus decreasing with the system size, in agreement with marked radicaloid character of the largest systems and with the T_1 state lower in energy with respect to the Q_1 state, as also obtained by the RAS-SF calculations. Since the relative stabilization of the HS with respect to the LS state is known to be strongly affected by the functional choice,[76–78] or more specifically by the fraction of exact-exchange,[79] we will next assess the performance of the PBE and PBE0 models, with the results shown in Fig. 7. When PBE is applied, the ground-state open-shell (singlet) solution collapsed to the closed-shell form for compounds 2- to 4-rhombene, but not for 5- and 6-rhombene. Thus, for 5- and 6-rhombene, the closed-shell singlet lies at 40 and 176 meV above in energy, respectively, with respect to the open-shell singlet state. This functional also provides for 5-rhombene the T_1 state separated by 174 meV from the open-shell state, an energy gap slightly overestimated with respect to both experimental (102 meV) and RAS-SF (139 meV) values. The Q_1 state is found much higher at 846 meV, close to the value obtained at the RAS-SF level (868 meV). In the case of 6-rhombene, the triplet lies above the singlet by 235 meV, which roughly represents a 3-fold overestimation of the RAS-SF result and evolves contrarily to the trend provided by RAS-SF and NEVPT2 results since ΔE_{ST} is found lower for 6-rhombene than for 5-rhombene. Note also that the ΔE_{ST} and ΔE_{SQ} energy differences are known to decrease for increasing

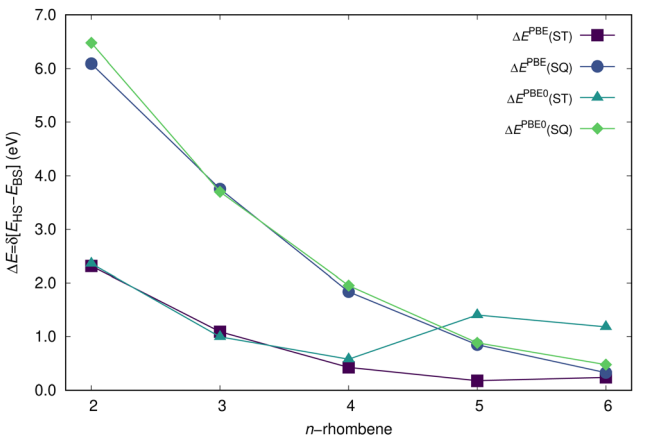

Fig. 7 Energy difference (in eV) between the low- and high-spin states of *n*-rhombenes, as calculated by DFT/def2-TZVP methods and spin-decontaminated as commented in the text.

Table 1 $\langle \hat{S}^2 \rangle$ calculated values for S_1, T_1, and Q_1 states of *n*-rhombenes, as calculated by DFT/def2-TZVP methods

	PBE			PBE0		
[*n*]	S_1	T_1	Q_1	S_1	T_1	Q_1
2	0.000	2.014	6.005	0.000	2.045	6.009
3	0.000	2.017	6.030	0.000	2.072	6.111
4	0.000	2.022	6.037	0.970	2.102	6.162
5	0.709	2.026	6.046	1.767	2.130	6.217
6	1.368	2.029	6.055	2.540	3.213	6.271

radicaloid nature, as it has been previously shown for *e.g.* linear and cyclic acenes.[63]

On the other hand, the PBE0 model predicted an open-shell ground-state for 4-rhombene, contrarily to experimental results, with the corresponding closed-shell state at 170 meV higher in energy. For the case of 5- and 6-rhombene, the closed-shell singlet lies as high as 630 and 1214 meV above in energy, respectively, with respect to the open-shell singlet. Additionally, the large spin contamination (see Table 1) is identified as the responsible factor for predicting the Q_1 state significantly more stable than the T_1 for 5-rhombene, as already anticipated by the RAS-SF results since the manifold of states was found very close in energy for the largest systems: ΔE_{ST} and ΔE_{SQ} are predicted to be 255 and 654 meV before applying the spin correction given by eqn (8), which modifies the values to 1403 and 882 meV, respectively. A similar situation is found for 6-rhombene, with values for ΔE_{ST} and ΔE_{SQ} of 1181 and 474 meV, respectively, once the spin correction is applied, see eqn (7) and (8). Finally, the evolution with the system size of the ΔE_{ST} and ΔE_{SQ} calculated values is presented in Fig. 7 taking into account the spin correction, with all the individual values for *n*-rhombenes at both PBE and PBE0 methods given as part of the ESI.†

3.4 Charged systems

We also investigated the energy associated to charge the systems, known as adiabatic ionization potential (AIP) or electron affinity (AEA) and calculated as energy differences between charged and neutral systems all at their respective optimized geometries: AIP = $E_{M}^{\bullet+} - E_M$ and AEA = $E_M - E_{M}^{\bullet-}$, with E_M being the energy of the neutral molecule and $E_{M}^{\bullet+}$ ($E_{M}^{\bullet-}$) the energy of the positively (negatively) charged molecule. The quasiparticle energy gap (QEG) is readily obtained as QEG = AIP − AEA. The corresponding vertical magnitudes are VIP (vertical ionization potential), VEA (vertical electron affinity), and VQEG (vertical quasiparticle energy gap) and are obtained at the ground-state geometries. We will employ the PBE0 and the PBE0-DH models to bracket the dependence of the values with the functional choice. Experimentally available AIP[80] and AEA[81] values for 2-rhombene (7.426 and 0.406 eV, respectively) will be used as test case to assess the accuracy of the DFT results. Whereas PBE0/def2-SVP gives values of 7.175 and 0.368 eV, respectively, the use of the larger def2-TZVP basis set produced values of 7.148 and 0.394 eV, showing a not very marked dependence of the results on the basis set size (furthermore PBE0/cc-pVTZ led to values of 7.135 and 0.356 eV,

Table 2 Energy differences (in eV) between positively or negatively charged and neutral *n*-rhombenes, as calculated by PBE0/def2-TZVP

	PBE0						FT-DFT					
[*n*]	AIP	VIP	AEA	VEA	AQEG	VQEG	AIP	VIP	AEA	VEA	AQEG	VQEG
2	7.148	7.231	0.394	0.280	6.754	6.950	6.749	6.768	0.652	0.613	6.097	6.156
3	6.076	6.127	1.559	1.502	4.517	4.625	5.834	5.842	1.638	1.621	4.197	4.221
4	5.604	5.615	2.137	2.125	3.467	3.491	5.371	5.374	2.177	2.170	3.194	3.205
5	5.679	5.726	2.166	2.101	3.513	3.625	5.113	5.115	2.497	2.493	2.616	2.622
6	5.568	5.585	2.276	2.237	3.292	3.349	4.945	4.947	2.711	2.709	2.233	2.238

respectively). The use of PBE0-DH instead leads to values of 7.271 and 0.284 eV (def2-SVP) and 7.256 and 0.334 eV (def2-TZVP) for AIP and AEA, respectively, slightly more influenced by basis sets effects due to the inclusion of the PT2 term in eqn (4). Choosing the PBE0 functional for its good trade-off between accuracy and computational cost, and looking at the evolution of these values with the system size, see Table 2, we observe a initial decreasing values as a function of n for all the energy magnitudes collected, up to some saturation for the 4- to 6-rhombene. Additionally, the difference between adiabatic and vertical values is reduced with the system size, which is rationalized by an enhanced rigidity of the molecular backbone for the largest systems studied. For the sake of completeness, we also used the FT-DFT method to observe a qualitatively similar evolution of the values with the system size.

The inner reorganization energy (Λ) for holes ($\Lambda_{h}{}^{\bullet+}$) or electrons ($\Lambda_{e}{}^{\bullet-}$), related to charge migration and transfer between neighbouring molecules[82,83] can also be obtained (in the hopping regime) from the following set of calculations:

$$\Lambda_{h(e)}{}^{\bullet\pm} = [E_{M}{}^{\bullet\pm}{}_{//M} - E_{M}{}^{\bullet\pm}] + [E_{M//M}{}^{\bullet}{}_{\pm} - E_{M}], \quad (11)$$

where $E_{M}{}^{\bullet\pm}{}_{//M}$ and $E_{M//M}{}^{\bullet}{}_{\pm}$ are now the energies of the charged molecule at the neutral geometry and that of the neutral at the charged geometry, respectively, with $E_{M}{}^{\bullet\pm}$ being the energy of the charged structures.[84,85] We will employ the PBE0 functional also here due to its accurate results for other conjugated (semiconducting) systems.[86–88] At the PBE0/def2-TZVP level, $\Lambda_{h}{}^{\bullet+}$ values of 157 and 103 meV are obtained for the smallest 2- and 3-rhombene members of the set of molecules, respectively, showing the typical evolution of these values with the system size (inversely proportional to the number of C atoms[89]) and favourably comparing with for instance circum(oligo)-acenes of increasing size, such as circumbenzene or coronene ($C_{24}H_{12}$) and circumtetracene ($C_{48}H_{18}$) with values of 127 and 57 meV, respectively, calculated before at the B3LYP/cc-pCVDZ level.[90] For the case of $\Lambda_{e}{}^{\bullet-}$, values of 225 and 147 meV are again calculated at the PBE0/def2-TZVP level, larger than those found before for $\Lambda_{h}{}^{\bullet+}$. The application of the PBE0-DH model led to $\Lambda_{h}{}^{\bullet+}$ ($\Lambda_{e}{}^{\bullet-}$) values of 182 and 114 meV (250 and 153 meV), thus confirming the trend found before with PBE0. Note that the reorganization energies of larger systems, following the expected evolution with the system size, would preclude the use of eqn (11) due to the gradual transition between the incoherent (hopping) and coherent (ballistic) transport regimes.[91] As a matter of illustration, for 6-rhombene values of Λ_{h^+} and Λ_{e^-} as low as 36 and 58 meV, respectively, are found.

4. Conclusions

We have systematically studied the electronic structure of increasingly larger rhombus-shaped molecules, or *n*-rhombenes, ranging from 2-rhombene ($C_{16}H_{10}$) to 6-rhombene ($C_{96}H_{26}$), due to the markedly increasing (poly)radicaloid character with the system size. The rationalization of that character is extensively done through the number and spatial extension of unpaired electrons, the fractional occupation of molecular orbitals, the frontier molecular orbital energy gap, and the total energy difference between singlet–triplet and singlet–quintet electronic states. The challenging electronic structure of these systems has prompted the use of multiconfigurational methods, such as RAS-*sr*DFT, RAS-SF, or NEVPT2, leading to: (i) a qualitative agreement between available experimental and theoretical results for the system size at which the transition from a closed-shell to an open-shell ground-state happens, and (ii) a quantitative and close agreement between theoretical and experimental results for the singlet–triplet energy difference for 5-rhombene. This agreement facilitates us to rely on the calculated singlet–triplet energy difference for 6-rhombene (not yet synthesized) which is lower than for 5-rhombene but still larger than the Landauer limit.

The quality of those wavefunction based results also served us to assess different DFT flavors (semi-local, hybrid, and double-hybrid functionals) for estimating the energy difference between different spin states (profoundly influenced by the spin contamination). For that situation, the spin contamination is alleviated by the use of the Yamaguchi's correction, which led to qualitatively correct results for 5-rhombene but not for 6-rhombene, disagreeing thus with results from wavefunction methods. The study of charged (monocationic and monoanionic) systems showed a decreasing (increasing) evolution of ionization potentials (electron affinity) with the system size, closing thus the quasiparticle energy gap as it was also expected due to their increasing (poly)radicaloid nature. The reorganization energy for hole or electron charge carrier transport in the hopping regime, for the smallest members of the family, show reasonably low values for those molecules to act as organic molecular semiconductors. On the other hand, the low-cost FT-DFT method can be considered as an alternative for dealing with (poly)radicaloids systems, providing fast and qualitatively correct results.

Data availability

The data that supports the findings of this study are available within the article [and its ESI†] or are available from the corresponding authors upon reasonable request.

Author contributions

M. E. S.-S. and R. B.-C. contributed equally to this work.

Conflicts of interest

There are no conflicts to declare.

Acknowledgements

This work is supported by projects PID2019-106114GB-I00 (''Ministerio de Ciencia e Innovación''), AICO/2021/093 and PROMETEO/2021/017 (''Generalitat Valenciana'').

References

1 W. Zeng and J. Wu, Open-shell graphene fragments, *Chem*, 2021, **7**(2), 358–386.
2 S. Moles Quintero, M. M. Haley, M. Kertesz and J. Casado, Polycyclic Hydrocarbons from [4n]Annulenes: Correlation versus Hybridization Forces in the Formation of Diradicaloids, *Angew. Chem., Int. Ed.*, 2022, **61**(44), e202209138.
3 Y. Gu, Z. Qiu and K. Müllen, Nanographenes and Graphene Nanoribbons as Multitalents of Present and Future Materials Science, *J. Am. Chem. Soc.*, 2022, **144**(26), 11499–11524.
4 F. de Souza, F. Pansini, A. R. Ambrozio, J. Freitas and W. L. Scopel, NMR spectral parameters of open-and closed-shell graphene nanoflakes: Orbital and hyperfine contributions, *Carbon*, 2022, **191**, 374–383.
5 I. Badía-Domínguez, S. Canola, V. Hernandez Jolin, J. T. Lopez Navarrete, J. C. Sancho-García and F. Negri, *et al.*, Tuning the Diradical Character of Indolocarbazoles: Impact of Structural Isomerism and Substitution Position. The, *J. Phys. Chem. Lett.*, 2022, **13**(26), 6003–6010.
6 D. G. de Oteyza and T. Frederiksen, Carbon-based nanostructures as a versatile platform for tunable π-magnetism, *J. Phys.: Condens. Matter*, 2022, **34**(44), 443001.
7 Z. Liu, S. Fu, X. Liu, A. Narita, P. Samorì and M. Bonn, *et al.*, Small Size, Big Impact: Recent Progress in Bottom-Up Synthesized Nanographenes for Optoelectronic and Energy Applications, *Adv. Sci.*, 2022, 2106055.
8 J. Fernández-Rossier and J. J. Palacios, Magnetism in graphene nanoislands, *Phys. Rev. Lett.*, 2007, **99**(17), 177204.
9 R. Ortiz, R. A. Boto, N. García-Martínez, J. C. Sancho-García, M. Melle-Franco and J. Fernández-Rossier, Exchange rules for diradical π-conjugated hydrocarbons, *Nano Lett.*, 2019, **19**(9), 5991–5997.
10 D. Jacob and J. Fernández-Rossier, Theory of intermolecular exchange in coupled spin-1 2 nanographenes, *Phys. Rev. B*, 2022, **106**(20), 205405.
11 A. Narita, X. Y. Wang, X. Feng and K. Müllen, New advances in nanographene chemistry, *Chem. Soc. Rev.*, 2015, **44**(18), 6616–6643.
12 S. Mishra, D. Beyer, K. Eimre, J. Liu, R. Berger and O. Groning, *et al.*, Synthesis and characterization of π-extended triangulene, *J. Am. Chem. Soc.*, 2019, **141**(27), 10621–10625.
13 S. Mishra, D. Beyer, K. Eimre, R. Ortiz, J. Fernández-Rossier and R. Berger, *et al.*, Collective all-carbon magnetism in triangulene dimers, *Angew. Chem.*, 2020, **132**(29), 12139–12145.
14 S. Mishra, J. Melidonie, K. Eimre, S. Obermann, O. Gröning and C. A. Pignedoli, *et al.*, On-surface synthesis of superheptazethrene, *Chem. Commun.*, 2020, **56**(54), 7467–7470.
15 S. Song, J. Su, M. Telychko, J. Li, G. Li and Y. Li, *et al.*, On-surface synthesis of graphene nanostructures with π-magnetism, *Chem. Soc. Rev.*, 2021, **50**(5), 3238–3262.
16 A. A. Ovchinnikov, Multiplicity of the ground state of large alternant organic molecules with conjugated bonds, *Theor. Chim. Acta*, 1978, **47**(4), 297–304.
17 E. H. Lieb, Two theorems on the Hubbard model, *Phys. Rev. Lett.*, 1989, **62**(10), 1201.
18 L. A. Agapito, N. Kioussis and E. Kaxiras, Electric-field control of magnetism in graphene quantum dots: Ab initio calculations, *Phys. Rev. B: Condens. Matter Mater. Phys.*, 2010, **82**(20), 201411.
19 C. N. Yeh and J. D. Chai, Role of Kekulé and non-Kekulé structures in the radical character of alternant polycyclic aromatic hydrocarbons: a TAODFT study, *Sci. Rep.*, 2016, **6**(1), 1–14.
20 S. Ganguly, M. Kabir and T. Saha-Dasgupta, Magnetic and electronic crossovers in graphene nanoflakes, *Phy. Rev. B*, 2017, **95**(17), 174419.
21 T. Förster and K. Kasper, Ein konzentrationsumschlag der fluoreszenz, *Z. Phys. Chem.*, 1954, **1**(5–6), 275–277.
22 L. Zhao, R. I. Kaiser, B. Xu, U. Ablikim, M. Ahmed and D. Joshi, *et al.*, Pyrene synthesis in circumstellar envelopes and its role in the formation of 2D nanostructures, *Nat. Astron*, 2018, **2**(5), 413–419.
23 F. P. Kinik, A. Ortega-Guerrero, D. Ongari, C. P. Ireland and B. Smit, Pyrenebased metal organic frameworks: from synthesis to applications, *Chem. Soc. Rev.*, 2021, **50**(5), 3143–3177.
24 J. Li, S. Chen, Z. Wang and Q. Zhang, Pyrene-fused Acenes and Azaacenes: Synthesis and Applications, *Chem. Rec.*, 2016, **16**(3), 1518–1530.
25 S. Mishra, X. Yao, Q. Chen, K. Eimre, O. Gröning and R. Ortiz, *et al.*, Large magnetic exchange coupling in rhombus-shaped nanographenes with zigzag periphery, *Nat. Chem.*, 2021, **13**(6), 581–586.
26 R. Ortiz and J. Fernández-Rossier, Probing local moments in nanographenes with electron tunneling spectroscopy, *Prog. Surf. Sci.*, 2020, **95**(4), 100595.
27 G. Salvitti, F. Negri, A. J. Pérez-Jiménez, E. San-Fabián, D. Casanova and J. C. Sancho-García, Investigating the (Poly) Radicaloid Nature of Real- World Organic Compounds with DFT-Based Methods, *J. Phys. Chem. A*, 2020, **124**(18), 3590–3600.
28 A. Omist, G. Ricci, A. Derradji, A. J. Pérez-Jiménez, E. San-Fabián and Y. Olivier, *et al.*, peri-Acenoacene molecules: tuning of the singlet and triplet excitation energies by modifying their radical character, *Phys. Chem. Chem. Phys.*, 2021, **23**(41), 24016–24028.

29 J. D. Chai, Density Functional Theory with Fractional Orbital Occupations, *J. Chem. Phys.*, 2012, **136**(15), 154104.
30 A. I. Krylov, Spin-flip configuration interaction: an electronic structure model that is both variational and size-consistent, *Chem. Phys. Lett.*, 2001, **350**(5), 522–530.
31 Y. Shao, M. Head-Gordon and A. I. Krylov, The spin–flip approach within time-dependent density functional theory: Theory and applications to diradicals. The, *J. Chem. Phys.*, 2003, **118**(11), 4807–4818.
32 A. I. Krylov, Spin-flip equation-of-motion coupled-cluster electronic structure method for a description of excited states, bond breaking, diradicals, and triradicals, *Acc. Chem. Res.*, 2006, **39**(2), 83–91.
33 D. Casanova, Restricted active space configuration interaction methods for strong correlation: Recent developments, *Wiley Interdiscip. Rev.: Comput. Mol. Sci.*, 2022, **12**(1), e1561.
34 D. Casanova, Short-range density functional correlation within the restricted active space CI method, *J. Chem. Phys.*, 2018, **148**(12), 124118.
35 N. Orms and A. I. Krylov, Singlet–triplet energy gaps and the degree of diradical character in binuclear copper molecular magnets characterized by spin-flip density functional theory, *Phys. Chem. Chem. Phys.*, 2018, **20**(19), 13127–13144.
36 M. E. Sandoval-Salinas, A. Carreras, J. Casado and D. Casanova, Singlet fission in spiroconjugated dimers, *J. Chem. Phys.*, 2019, **150**(20), 204306.
37 J. D. Chai, Thermally-assisted-occupation density functional theory with generalized-gradient approximations, *J. Chem. Phys.*, 2014, **140**(18), 18A521.
38 S. Grimme and A. Hansen, A practicable real-space measure and visualization of static electron-correlation effects, *Angew. Chem., Int. Ed.*, 2015, **54**(42), 12308–12313.
39 C. A. Bauer, A. Hansen and S. Grimme, The fractional occupation number weighted density as a versatile analysis tool for molecules with a complicated electronic structure, *Chem. – Eur. J.*, 2017, **23**(25), 6150–6164.
40 D. Casanova and A. I. Krylov, Spin-flip methods in quantum chemistry, *Phys. Chem. Chem. Phys.*, 2020, **22**(8), 4326–4342.
41 J. P. Perdew, K. Burke and M. Ernzerhof, Generalized gradient approximation made simple, *Phys. Rev. Lett.*, 1996, **77**(18), 3865.
42 C. Adamo and V. Barone, Toward reliable density functional methods without adjustable parameters: The PBE0 model. The, *J. Chem. Phys.*, 1999, **110**(13), 6158–6170.
43 E. Brémond and C. Adamo, Seeking for parameter-free double-hybrid functionals: the PBE0-DH model, *J. Chem. Phys.*, 2011, **135**(2), 024106.
44 E. Brémond, I. Ciofini, J. C. Sancho-García and C. Adamo, Nonempirical double-hybrid functionals: An effective tool for chemists, *Acc. Chem. Res.*, 2016, **49**(8), 1503–1513.
45 J. C. Sancho-Garcia, E. Brémond, A. Pérez-Jiménez, I. Ciofini and C. Adamo, Non-empirical double-hybrid density functionals as reliable tools for electronic structure calculations, *Electron. Struct.*, 2022, **4**(4), 043001.
46 K. Yamaguchi, H. Fukui and T. Fueno, Molecular orbital (MO) theory for magnetically interacting organic compounds. Ab-initio MO calculations of the effective exchange integrals for cyclophane-type carbene dimers, *Chem. Lett.*, 1986, (4), 625–628.
47 K. Yamaguchi, Y. Takahara, T. Fueno and K. N. Houk, Extended Hartree- Fock (EHF) theory of chemical reactions, *Theor. Chim. Acta*, 1988, **73**(5), 337–364.
48 S. Yamanaka, M. Okumura, M. Nakano and K. Yamaguchi, EHF theory of chemical reactions Part 4. UNO CASSCF, UNO CASPT2 and R(U)HF coupled-cluster (CC) wavefunctions, *J. Mol. Struct.: THEOCHEM*, 1994, **310**, 205–218.
49 S. Grimme, J. G. Brandenburg, C. Bannwarth and A. Hansen, Consistent structures and interactions by density functional theory with small atomic orbital basis sets, *J. Chem. Phys.*, 2015, **143**(5), 054107.
50 J. Tao, J. P. Perdew, V. N. Staroverov and G. E. Scuseria, Climbing the density functional ladder: Nonempirical meta–generalized gradient approximation designed for molecules and solids, *Phys. Rev. Lett.*, 2003, **91**(14), 146401.
51 F. Weigend and R. Ahlrichs, Balanced basis sets of split valence, triple zeta valence and quadruple zeta valence quality for H to Rn: Design and assessment of accuracy, *Phys. Chem. Chem. Phys.*, 2005, **7**(18), 3297–3305.
52 F. Neese, Software update: the ORCA program system, version 4.0, *Wiley Interdiscip. Rev.: Comput. Mol. Sci.*, 2018, **8**(1), e1327.
53 M. D. Hanwell, D. E. Curtis, D. C. Lonie, T. Vandermeersch, E. Zurek and G. R. Hutchison, Avogadro: an advanced semantic chemical editor, visualization, and analysis platform, *J. Cheminf.*, 2012, **4**(1), 1–17.
54 S. Kossmann and F. Neese, Comparison of two efficient approximate Hartee– Fock approaches, *Chem. Phys. Lett.*, 2009, **481**(4–6), 240–243.
55 F. Weigend, Hartree–Fock exchange fitting basis sets for H to Rn, *J. Comput. Chem.*, 2008, **29**(2), 167–175.
56 E. Epifanovsky, A. T. B. Gilbert, X. Feng, J. Lee, Y. Mao and N. Mardirossian, *et al.*, Software for the frontiers of quantum chemistry: An overview of developments in the Q-Chem 5 package, *J. Chem. Phys.*, 2021, **155**(8), 084801.
57 R. W. Havenith, J. H. Van Lenthe, F. Dijkstra and L. W. Jenneskens, Aromaticity of Pyrene and Its Cyclopentafused Congeners Resonance and NICS Criteria. An Ab Initio Valence Bond Analysis in Terms of Kekulé Resonance Structures, *J. Phys. Chem. A*, 2001, **105**(15), 3838–3845.
58 É. Brémond, M. Savarese, N. Q. Su, A. J. Pérez-Jiménez, X. Xu and J. C. Sancho- García, *et al.*, Benchmarking density functionals on structural parameters of small-/medium-sized organic molecules, *J. Chem. Theory Comput.*, 2016, **12**(2), 459–465.
59 M. Kertesz, C. H. Choi and S. Yang, Conjugated polymers and aromaticity, *Chem. Rev.*, 2005, **105**(10), 3448–3481.
60 J. C. Sancho-García and A. J. Pérez-Jiménez, Improved accuracy with medium cost computational methods for the evaluation of bond length alternation of increasingly long oligoacetylenes, *Phys. Chem. Chem. Phys.*, 2007, **9**(44), 5874–5879.
61 S. R. Langhoff, Theoretical infrared spectra for polycyclic aromatic hydrocarbon neutrals, cations, and anions, *J. Phys. Chem.*, 1996, **100**(8), 2819–2841.

62 C. S. Wu and J. D. Chai, Electronic properties of zigzag graphene nanoribbons studied by TAO-DFT, *J. Chem. Theory Comput.*, 2015, **11**(5), 2003–2011.
63 A. Pérez-Guardiola, M. E. Sandoval-Salinas, D. Casanova, E. San-Fabián, A. J. Pérez-Jiménez and J. C. Sancho-Garcia, The role of topology in organic molecules: origin and comparison of the radical character in linear and cyclic oligoacenes and related oligomers, *Phys. Chem. Chem. Phys.*, 2018, **20**(10), 7112–7124.
64 H. J. Huang, S. Seenithurai and J. D. Chai, TAO-DFT study on the electronic properties of diamond-shaped graphene nanoflakes, *Nanomaterials*, 2020, **10**(6), 1236.
65 D. Doehnert and J. Koutecky, Occupation numbers of natural orbitals as a criterion for biradical character. Different kinds of biradicals, *J. Am. Chem. Soc.*, 1980, **102**(6), 1789–1796.
66 J. P. Malrieu and G. Trinquier, Can a topological approach predict spinsymmetry breaking in conjugated hydrocarbons?, *J. Phys. Chem. A*, 2016, **120**(48), 9564–9578.
67 D. Jacob, R. Ortiz and J. Fernández-Rossier, Renormalization of spin excitations and Kondo effect in open-shell nanographenes, *Phys. Rev. B*, 2021, **104**(7), 075404.
68 R. Landauer, Irreversibility and heat generation in the computing process, *IBM J. Res. Dev.*, 1961, **5**(3), 183–191.
69 C. Angeli, R. Cimiraglia, S. Evangelisti, T. Leininger and J. P. Malrieu, Introduction of N-electron valence states for multireference perturbation theory, *J. Chem. Phys.*, 2001, **114**(23), 10252–10264.
70 C. Angeli, R. Cimiraglia and J. P. Malrieu, N-electron valence state perturbation theory: a fast implementation of the strongly contracted variant, *Chem. Phys. Lett.*, 2001, **350**(3–4), 297–305.
71 C. Angeli, R. Cimiraglia and J. P. Malrieu, N-electron valence state perturbation theory: A spinless formulation and an efficient implementation of the strongly contracted and of the partially contracted variants, *J. Chem. Phys.*, 2002, **117**(20), 9138–9153.
72 B. Shi, D. Nachtigallova, A. J. Aquino, F. B. Machado and H. Lischka, Highlevel theoretical benchmark investigations of the UV-vis absorption spectra of paradigmatic polycyclic aromatic hydrocarbons as models for graphene quantum dots, *J. Chem. Phys.*, 2019, **150**(12), 124302.
73 M. El Khatib, S. Evangelisti, T. Leininger and G. L. Bendazzoli, A theoretical study of closed polyacene structures, *Phys. Chem. Chem. Phys.*, 2012, **14**(45), 15666–15676.
74 L. Cusinato, S. Evangelisti, T. Leininger and A. Monari, The Electronic Structure of Graphene Nanoislands: A CAS-SCF and NEVPT2 Study, *Adv. Condens. Matter Phys.*, 2018, **2018**, 9097045.
75 V. N. Staroverov, G. E. Scuseria, J. Tao and J. P. Perdew, Comparative assessment of a new nonempirical density functional: Molecules and hydrogen-bonded complexes, *J. Chem. Phys.*, 2003, **119**(23), 12129–12137.
76 M. Swart and M. Gruden, Spinning around in transition-metal chemistry, *Acc. Chem. Res.*, 2016, **49**(12), 2690–2697.
77 S. Song, M. C. Kim, E. Sim, A. Benali, O. Heinonen and K. Burke, Benchmarks and reliable DFT results for spin gaps of small ligand Fe (II) complexes, *J. Chem. Theory Comput.*, 2018, **14**(5), 2304–2311.
78 L. Rousseau, E. Brémond and G. Lefèvre, Assessment of the ground spin state of iron (I) complexes: insights from DFT predictive models, *New J. Chem.*, 2018, **42**(10), 7612–7616.
79 M. Reiher, O. Salomon and B. Artur Hess, Reparameterization of hybrid functionals based on energy differences of states of different multiplicity, *Theor. Chem. Acc.*, 2001, **107**(1), 48–55.
80 J. W. Hager and S. C. Wallace, Two-laser photoionization supersonic jet mass spectrometry of aromatic molecules, *Anal. Chem.*, 1988, **60**(1), 5–10.
81 N. Ando, S. Kokubo, M. Mitsui and A. Nakajima, Photoelectron spectroscopy of pyrene cluster anions,(pyrene) n-(n= 1–20), *Chem. Phys. Lett.*, 2004, **389**(4–6), 279–283.
82 V. Coropceanu, J. André, M. Malagoli and J. Brédas, The Role of Vibronic Interactions on Intramolecular and Intermolecular Electron Transfer in π-Conjugated Oligomers, *Theor. Chem. Acc.*, 2003, **110**(2), 59–69.
83 F. C. Grozema and L. D. Siebbeles, Mechanism of Charge Transport in Self- Organizing Organic Materials, *Int. Rev. Phys. Chem.*, 2008, **27**(1), 87–138.
84 S. F. Nelsen, S. C. Blackstock and Y. Kim, Estimation of Inner Shell Marcus Terms for Amino Nitrogen Compounds by Molecular Orbital Calculations, *J. Am. Chem. Soc.*, 1987, **109**(3), 677–682.
85 J. L. Brédas, D. Beljonne, V. Coropceanu and J. Cornil, Charge-Transfer and Energy-Transfer Processes in π-Conjugated Oligomers and Polymers: A Molecular Picture, *Chem. Rev.*, 2004, **104**(11), 4971–5004.
86 R. S. Sánchez-Carrera, V. Coropceanu, D. A. da Silva Filho, R. Friedlein, W. Osikowicz and R. Murdey, *et al.*, Vibronic Coupling in the Ground and Excited States of Oligoacene Cations, *J. Phys. Chem. B*, 2006, **110**(38), 18904–18911.
87 J. C. Sancho-García, Assessment of Density-Functional Models for Organic Molecular Semiconductors: The Role of Hartree–Fock Exchange in Charge-Transfer Processes, *Chem. Phys.*, 2007, **331**(2), 321–331.
88 C. Sutton, J. S. Sears, V. Coropceanu and J. L. Brédas, Understanding the Density Functional Dependence of DFT-Calculated Electronic Couplings in Organic Semiconductors, *J. Phys. Chem. Lett.*, 2013, **4**(6), 919–924.
89 A. Devos and M. Lannoo, Electron-phonon coupling for aromatic molecular crystals: Possible consequences for their superconductivity, *Phys. Rev. B: Condens. Matter Mater. Phys.*, 1998, **58**(13), 8236.
90 J. C. Sancho-García and A. J. Pérez-Jiménez, Charge-transport properties of prototype molecular materials for organic electronics based on graphene nanoribbons, *Phys. Chem. Chem. Phys.*, 2009, **11**(15), 2741–2746.
91 A. J. Perez-Jimenez and J. C. Sancho-García, Using circumacenes to improve organic electronics and molecular electronics: design clues, *Nanotechnology*, 2009, **20**(47), 475201.